Biophysical Journal
Article

Biophysical Society

HEXIM1 Diffusion in the Nucleus Is Regulated by Its Interactions with Both 7SK and P-TEFb

Alessandro Furlan,[1,*] Mariano Gonzalez-Pisfil,[1] Aymeric Leray,[2] Dorian Champelovier,[1] Mélanie Henry,[1] Corentin Le Nézet,[1] Oliver Bensaude,[3] Marc Lefranc,[1] Thorsten Wohland,[4] Bernard Vandenbunder,[1] Gabriel Bidaux,[1,5] and Laurent Héliot[1,*]

[1]University of Lille, CNRS, UMR 8523, PhLAM Laboratoire de Physique des Lasers, Atomes et Molécules, Lille, France; [2]Laboratoire Interdisciplinaire Carnot de Bourgogne, UMR 6303 CNRS, Université de Bourgogne Franche Comté, Dijon, France; [3]Institut de biologie de l'Ecole normale supérieure (IBENS), Ecole normale supérieure, CNRS, INSERM, PSL Research University, Paris, France; [4]Departments of Biological Sciences and Chemistry, Center for Bioimaging Sciences, National University of Singapore, Singapore, Singapore; and [5]INSERM UMR 1060, CarMeN laboratory, Univ Lyon1, IHU OPERA, Hôpital Louis Pradel, Hospices Civils de Lyon, Lyon, France

ABSTRACT How nuclear proteins diffuse and find their targets remains a key question in the transcription field. Dynamic proteins in the nucleus are classically subdiffusive and undergo anomalous diffusion, yet the underlying physical mechanisms are still debated. In this study, we explore the contribution of interactions to the generation of anomalous diffusion by the means of fluorescence spectroscopy and simulation. Using interaction-deficient mutants, our study indicates that HEXIM1 interactions with both 7SK RNA and positive transcription elongation factor b are critical for HEXIM1 subdiffusion and thus provides evidence of the effects of protein-RNA interaction on molecular diffusion. Numerical simulations allowed us to establish that the proportions of distinct oligomeric HEXIM1 subpopulations define the apparent anomaly parameter of the whole population. Slight changes in the proportions of these oligomers can lead to significant shifts in the diffusive features and recapitulate the modifications observed in cells with the various interaction-deficient mutants. By combining simulations and experiments, our work opens new prospects in which the anomaly α coefficient in diffusion becomes a helpful tool to infer alterations in molecular interactions.

SIGNIFICANCE Nuclear molecules are classically subdiffusive, and molecular crowding has often been incriminated among various putative reasons. The potential contribution of intermolecular interactions was proposed but has generally been neglected. To move the field forward, we tackled this issue by focusing on a complex of RNA and proteins. We unveiled the key role of 7SK RNA and P-TEFb binding to HEXIM1 in driving the anomalous diffusion of the latter. To our best knowledge, this is the first direct evidence of the effect of interactions between RNAs and proteins on molecular diffusion in vivo. Our study also shows that the anomaly coefficient can be used as a simple and robust tool to report on molecular interactions involved in various important biological questions.

INTRODUCTION

Despite the lack of bona fide internal subcompartments, the nucleus of eukaryotic cells is spatially organized (1). The nucleolus represents the most obvious example and consists of DNA, RNA, and proteins gathered in a structure readily observable by microscopy. Besides, DNA is organized in chromosome territories in a nonrandom and dynamic manner (2). Another key feature in the nuclear architecture, possibly affecting its exploration by diffusible molecules, is the heterogeneous condensation of chromatin in heterochromatin and euchromatin regions (3). Within this frame, processes such as replication or transcription are dynamically regulated by soluble molecules (RNA and proteins), which may assemble within RNP particles and must navigate in this crowded nuclear space. Indeed, macromolecules can be highly concentrated in cells, up to 400 g/L, and intracellular fluids can thus be regarded as crowded (4). The diffusion of nuclear proteins in this heterogenous nucleoplasmic environment plays a key role in their target search (5,6). When analyzed by quantitative microscopy approaches, nuclear molecules do not diffuse freely, but they typically

Submitted July 29, 2019, and accepted for publication September 9, 2019.

*Correspondence: alessandro.furlan@univ-lille.fr or laurent.heliot@univ-lille.fr

Alessandro Furlan and Mariano Gonzalez-Pisfil participated equally to the work.

Gabriel Bidaux and Laurent Héliot share senior authorship.

Editor: Tom Misteli.

https://doi.org/10.1016/j.bpj.2019.09.019

display a power-law increase of their mean-square displacement (MSD) as a function of time t, MSD $\propto t^{\alpha}$ (7), characterized by an anomaly coefficient $\alpha < 1$. This means that the motion of nuclear molecules is time and length scale dependent. On short time and length scales, nuclear molecules diffuse almost freely, but on longer scales, interactions with obstacles become significant, and diffusion is restricted. Such hindered diffusion may contribute in biology to the control of the diffusion distance and the existence of local concentration gradients, which have been measured experimentally and participate in the regulation of biological functions (8). Even if it seems counterintuitive, simulations have shown that anomalous diffusion can outperform Brownian diffusion in finding a target (9).

The underlying biological reasons for nuclear protein anomalous diffusion are still poorly understood and debated (10,11). Even if the viscosity of the intracellular environment can affect molecular diffusion (12), many other mechanisms govern intracellular diffusion far beyond the Stokes-Einstein relationship. The anomalous diffusion of molecules in the nucleus may be driven by hydrodynamic forces and steric hindrance of the environment (10,13–15). Models for the role of macromolecular crowding in gene transcription modulation have been proposed (6,16). Yet, the extent of the contribution of crowding to cellular anomalous diffusion remains controversial, and other mechanisms such as molecular interactions have been proposed to participate in anomalous diffusion in living cells (17).

To assess the putative involvement of molecular interactions in the generation of anomalous diffusion, we used both experimental and simulation approaches. We focused our attention on HEXIM1, a protein regulating the transcription pause release. Most metazoan genes undergo a transcription pause after the initiation of transcription and require the activity of positive transcription elongation factor b (P-TEFb) to resume transcription. P-TEFb is a heterodimer of cyclin-dependent kinase 9 (CDK9) associated with cyclin T1 (CT1) or cyclin T2 in a minority of complexes. The CT1 amount in cells has been estimated to be around 3000 units per U20S cell (18), and CT1 is thus a limiting factor given the tens of thousands of transcription start sites identified in the human genome (19). How its motility is regulated between genes, which it controls over time, represents a question of interest in the transcription field. P-TEFb was reported to interact with the 7SK noncoding RNA and HEXIM1 protein in a ribonucleoprotein called 7SK RNP, with both partners contributing to the inhibition of its kinase activity (20–22). Dynamic remodeling of this RNP was shown to regulate P-TEFb activity (23). Beyond sequestering P-TEFb in its inactive form in the RNP, HEXIM1 has been shown to participate in the recruitment of P-TEFb to enhancer regions (24). Interaction of the large P-TEFb/HEXIM1/7SK complex with histones, by affecting a methylase activity in the 7SK RNP, can destabilize 7SK RNA and allow P-TEFb activation in situ (25). In this context, HEXIM1 plays a key role as a hub connecting both RNAs and proteins (26). HEXIM1 thus represents a good candidate to evaluate the impact of different interactions on diffusion.

Thanks to advances in fluorescence microscopy, several approaches have emerged to study molecular dynamics and interactions in the single live-cell context (27–29). Fluorescence correlation spectroscopy (FCS) and its variants such as fluorescence cross correlation spectroscopy and spot variation FCS have been applied to infer from fluorescence intensity fluctuations information on molecular dynamics in cells (27,30,31). In this study, we assessed molecular diffusion using FCS with engineered fluorescent fusion proteins. HEXIM1 mutants deficient for interactions with 7SK RNA or P-TEFb, as well as the knock-down of HEXIM1 partners, indicate that HEXIM1 anomalous diffusion was dictated by its interactions. Subsequent numerical simulations were performed, which allowed us to 1) demonstrate the generation of diffusive anomaly by mixing particles, which diffuse with distinct diffusion coefficients, and 2) recapitulate the diffusive anomaly dependent on the presence of distinct HEXIM1 oligomers in vivo.

MATERIALS AND METHODS

Cell line culture

U2OS cell line (from the American Type Culture Collection, Manassas, VA) was cultured in DMEM medium (Gibco Laboratories, Gaithersburg, MD) supplemented with 10% FCS (vol/vol) and penicillin/streptomycin (100 mg/mL). For live-cell imaging, cells were plated on 35-mm glass-bottom dishes (Ibidi, CliniSciences, Nanterre, France), filled with L-15 medium without Phenol Red (Life Technologies, Carlsbad, CA), and incubated at 37°C in a thermostatic chamber (Life Imaging Services, Basel, Switzerland).

Cloning

pmEGFPN1 was derived from pEGFPN1 by directed mutagenesis. HEXIM1 wild-type or variants DNA coding sequence was inserted after PCR in the multicloning site of the pmEGFP-N1 vector. The linker length was set to a minimum of eight amino acids to allow enough flexibility and minimal impairment of interaction interfaces. After a 0.8% (w/vol) agarose-gel extraction of specific DNA bands (Wizard SV gel and PCR Clean-Up System; Promega, Madison, WI), PCR products and recipient pmEGFPN1 vectors were digested with High Fidelity (New England BioLabs, Ipswich, MA) at 37°C overnight. Digested PCR products and recipient pmEGFPN1 vectors were ligated with T4 ligase (New England BioLabs) at 16°C overnight and transformed in JM109 chemocompetent bacteria (New England BioLabs). Final plasmids were extracted and sequenced before transfection experiments.

Transfection

500 ng of plasmid were transfected in 100,000 cells with Fugene Transfection Reagent (Promega, Madison, WI) following the manufacturer recommendations. For control mEGFP, 100 ng of plasmid were sufficient for a proper transfection.

RNA interference was achieved by using small interfering RNA (siRNA) directed against CT1 (AGUGGCAGGUGGAGAUAAA and GCGCGAAG CAUGCAGAAGA), CDK9 (GGCCAGAAGCGGAAGGUGA and GGA CAUGAAGGCUGCUAAU), 7SK (UGAGAGCUUGUUUGGAGGU and AAGCUCAAGGUCCAUUUGU) (32,33), or SR-CL000-005 as control

siRNAs (Kaneka Eurogentec, Seraing, Belgium). siRNA transfection was carried out with the HiperFect Reagent (QIAGEN, Germantown, MD), according to the manufacturer recommendations.

Confocal microscopy

Fluorescent cell images were obtained on a TCS SP5 X (Leica Microsystems, Wetzlar, Germany) confocal head with the single molecule detection upgrade, mounted on an inverted microscope (DMI6000; Leica Microsystems). In all experiments, a 63×/1.2 water immersion objective and the 488-nm line of an Argon-Ion laser were used. Fluorescence was recorded with a photomultiplier tube, and the microscope was controlled with LAS AF (Leica Microsystems) software.

FCS

FCS measurements were performed on the confocal microscope detailed in the previous section. Fluorescence was detected through a 525/50 single bandpass filter (Semrock, Rochester, NY) on a single photon avalanche photodiode (Micro Photon Devices, Bolzano, Italy). Single photon events were recorded by a HydraHarp 400 time-correlated single photon counting module (PicoQuant, Berlin, Germany). Measurements were controlled with the softwares LAS AF (Leica Microsystems) and SymphoTime (PicoQuant). Acquisition time for one FCS measurement was 30 s. Time-resolved raw data were exported, and autocorrelated data were generated with the software F2COR (34). Autocorrelated data were then imported in the software QuickFit 3.0 (DKFZ, Heidelberg, Germany) and fitted in batch with an anomalous three-dimensional diffusion model.

FCS data analysis

The observation volume V was calibrated with a 10 nM concentration solution of ATTO488 in water. The number N of molecules in this observation volume was inferred from the autocorrelation function (ACF) with the following:

$$N = \frac{1}{G(0)}, \tag{1}$$

and the observation volume V was determined with the following:

$$V = \frac{n}{C} = \frac{N}{N_A.C} = \frac{1}{G(0).N_A.C}, \tag{2}$$

n being the number of moles and N_A being the Avogadro number.

Subsequently, the concentration of mEGFP-tagged chimera in the observation volume was calculated with the following:

$$C = \frac{N}{N_A.V} = \frac{1}{G(0).N_A.V}. \tag{3}$$

When freely diffusing molecules in a three-dimensional volume are probed with a three-dimensional Gaussian laser with $1/e^2$ lateral and axial widths of w_o and z_0, the ACF $G(\tau)$ can be expressed analytically (35):

$$G(\tau) = \frac{1}{N}\left(\frac{1}{1+\left(\frac{\tau}{\tau_D}\right)}\right)\left(\frac{1}{\sqrt{1+\frac{w_0^2}{z_0^2}\left(\frac{\tau}{\tau_D}\right)}}\right), \tag{4}$$

where N is the number of molecules, and τ_D is the characteristic residence time.

For anomalous diffusion, the MSD is no longer linearly dependent on time, but it evolves proportionally with time to the power of α. In this case, the ACF becomes the following (7):

$$G(\tau) = \frac{1}{N}\left(\frac{1}{1+\left(\frac{\tau}{\tau_D}\right)^{\alpha}}\right)\left(\frac{1}{\sqrt{1+\frac{w_0^2}{z_0^2}\left(\frac{\tau}{\tau_D}\right)^{\alpha}}}\right). \tag{5}$$

The fitting of the ACFs was done with the trust region reflective least-squares algorithm. To evaluate the goodness of the fit, we used the sum of the squared error.

Generation of FCS simulations

Our FCS simulations were based on a Monte Carlo method written in C and detailed in (36). Briefly, particles were uniformly and randomly distributed inside a sphere of radius r = 3 μm. Particle displacements within this volume were based on random walks generated with the following procedure. The step size s between two jumps was sampled according to a Gaussian random generator with mean 0 and SD $\sigma = (6D\Delta_t)^{1/2}$, where D is the diffusion coefficient, and Δ_t is the sampling time of FCS simulations (0.4 μs). The deflection angle was completely isotropic, meaning that the azimuthal scattering angle was assumed uniformly distributed over [0, 2π], and the polar angle was uniformly distributed over [0, π] and then randomized as $\theta = \pi\xi$, where ξ is a random variable uniformly distributed over the interval [0, 1]. Each particle that exited the sphere was replaced by a new one, which was randomly generated at the surface of the sphere, to keep the number of particles constant inside the volume. When the particle was inside the focal volume of the microscope objective, the fluorescence intensity was calculated according to (36), and the corresponding ACF were calculated. Because the sampling time of 0.4 μs is much larger than the rotational correlation time, the orientation of the particle inside the focal volume was not taken into account, implying that both the phase and polarization effects were ignored. Each particle diffused during a lag time of 0.1 s, and then another particle was launched until the total number of particles N_{tot} was reached; N_{tot} was deduced from the concentration c from $N_{tot} = cN_A4/3\pi r^3$, where N_A is Avogadro's constant. This process was repeated 1000 times to improve the signal/noise ratio of the obtained autocorrelation curve. To ensure statistical reliability of the results, five autocorrelation curves were generated.

When multiple populations are simulated, both the fraction and the diffusion coefficient of each population are required. For the first population of fraction f_1 (corresponding to a number of particles $N_1 = f_1 * N_{tot}$) and diffusion coefficient D_1, the diffusion process previously described was executed until N_1 was reached. Then, the second population of fraction f_2 and D_2 was considered and so on. As previously mentioned, this process was repeated 1000 times to obtain a reliable autocorrelation curve, and finally, five autocorrelation curves were generated for each condition. Note that each particle is completely independent, meaning that all particle interactions are ignored.

Simulations were performed according to the experimental conditions previously described (36). A 514-nm continuous wave laser of power 100 μW was focused through a 63× water immersion objective (NA = 1.2) into a solution of diluted fluorophores with an absorption cross-section of 2.2×10^{-20} m^2 and a quantum yield of 0.98. If not stated otherwise, we used a fluorophore concentration of 4 nM corresponding to 272 particles inside the considered volume. The emitted fluorescence was then filtered by a 50-μm diameter pinhole and collected by a sensitive detector. Simulation data were directly processed by EasyFCS, a homemade

software developed with MATLAB and Statistics Toolbox (version R2016B; The MathWorks, Natick, MA). This software is available free of charge on request (contact: aymeric.leray@u-bourgogne.fr).

Statistical analysis

Each experiment was repeated at least three times, measurements were carried out in five different spots of different cells with a cumulative n > 125 for each condition, and the results were expressed as mean ± standard deviation (SD). The data were analyzed using the software GraphPad Prism (GraphPad Software, San Diego, CA). For statistical analysis of experimental results, mean values were compared with the wild-type condition using unpaired *t*-test with Welch's corrected test. Statistical significance was considered to be reached for $p < 0.05$. Matching experimental results with the closest simulations was performed using ANOVA.

RESULTS

FCS reveals subdiffusion of proteins involved in the P-TEFb complex

We first quantitatively assessed the diffusion of HEXIM1 and proteins of the P-TEFb in the nucleoplasm of U2OS cells. FCS experiments measure changes in fluorescence occurring in a voxel illuminated by a laser beam and enable the biophysical characterization of the diffusion of fluorescent molecules in this volume. Proteins of interest were fused to monomeric enhanced green fluorescent protein (mEGFP). mEGFP combines good quantum yield and photostability, even when compared to more recent variants (37), and photostability is an important feature to extract high-quality data on diffusion from FCS experiments. Moreover, mEGFP bears a mutation greatly reducing the tendency of green fluorescent protein to dimerize, which may have biased the experiments by modifying its molecular brightness (38). We then measured by FCS the diffusion of mEGFP tagged to either HEXIM1, CT1, or CDK9 (the P-TEFb subunits) or the NELFs dichlorobenzimidazole 1-β-D-ribofuranoside sensibility-inducing factor (DSIF) and negative elongation factor (NELF), which are P-TEFb targets. The diffusion of monomeric mEGFP and mEGFP fused to mNeptune (to double its molecular weight without affecting its molecular brightness (mEGFP-mNeptune)) was assessed as a control. The ACF of fluorescence intensity fluctuations was then calculated and fitted with an anomalous model as previously described (39). Mobile nuclear proteins actually do not diffuse freely, and their diffusion can be analyzed with the anomalous model, described in more detail in the Materials and Methods. Moreover, we chose this phenomenological anomalous model because it does not require knowing the number of distinct diffusive subpopulations, which is hard to predict for biological samples. The calculated residence time (τ_D), number of molecules (N), and anomaly coefficient (α) of the diffusion of each mEGFP chimera globally represent the diffusive properties of several subpopulations of unknown mole fraction and diffusion coefficient. Examples of FCS data and fits are shown in Fig. 1 *A* for mEGFP, mEGFP-mNeptune, and mEGFP-tagged CT1, CDK9, or HEXIM1. Fit residuals were low as a reflection of the quality of the fitting method (Fig. S1 *A*). Residence times (τ_D) were plotted as a function of α, with the spot size being proportional to the apparent

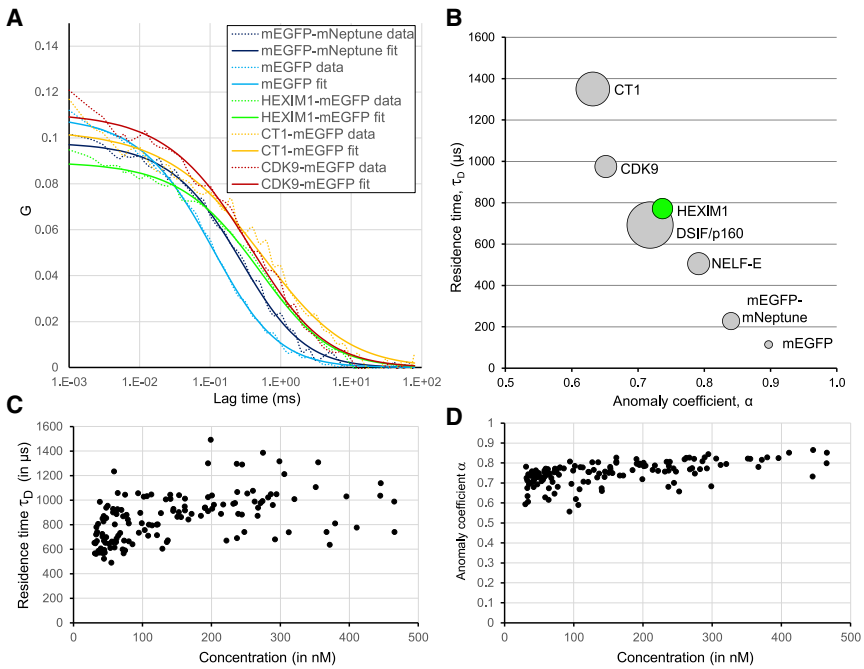

FIGURE 1 Fluorescence correlation spectroscopy (FCS) reveals the subdiffusion of proteins involved in the P-TEFb complex. (*A*) Nuclei of cells transfected with free mEGFP, mEGFP-mNeptune, or mEGFP-tagged HEXIM1, cyclin T1 (CT1) or cyclin-dependent kinase 9 (CDK9) were analyzed for fluorescence fluctuations by FCS. ACFs calculated from the fluctuations are plotted as a function of the lag time (in ms). (*B*) Residence times τ_D are plotted as a function of anomaly coefficient α, with a spot size proportional to the apparent molecular weight of considered proteins. The following molecular weights were considered for the mEGFP fusion proteins: 187 kDa for DSIF/p160, 108 kDa for CT1, 73 kDa for CDK9, 70 kDa for NELF-E, 68 kDa for HEXIM1, 54 kDa for mEGFP-mNeptune, and 27 kDa for mEGFP alone. The Table S1 gathers the mean values and SDs for the various proteins. (*C* and *D*) Cells transfected with mEGFP-HEXIM1 and expressing various levels of fluorescence were analyzed by FCS. The residence times τ_D (*C*) and anomaly coefficients α (*D*) were calculated for a range of concentrations from 20 to 500 nM. Each measurement is represented by a single dot (n = 143). To see this figure in color, go online.

molecular weight (Fig. 1 *B*). mEGFP-mNeptune and mEGFP displayed a diffusion close to Brownian diffusion, with an α between 0.8 and 0.9. All tagged transcription-related proteins had a subdiffusive behavior, with NELF-E subunit being the most diffusive and CT1 the most subdiffusive (Fig. 1 *B*; Table S1). DSIF/p160 diffuses similarly to HEXIM1, although it is quite larger (187 vs 68 kDa), whereas proteins with similar molecular weight (such as CDK9-mEGFP and NELF-mEGFP) display very divergent diffusive parameters (Figs. 1 *B*, S1 *B*, and S1 *C*). We carried out a correlation analysis, which showed that α and τ_D are inversely correlated (correlation factor $= -0.95$; p-value $= 0.0008$), whereas none of these diffusive features significantly correlated with molecular weight (Figs. S1 *D* and S1 *E*). The α for CT1 was estimated to be 0.63 ± 0.02, in agreement with previous measurements of CT1-Dendra2 diffusion in U20S cells by single particle tracking photoactivation localization microscopy with an acquisition frame rate of 100 Hz (5). The accuracy of FCS relies on the study of an optimal number of molecules N in the effective FCS volume during the recording time period. We anticipated that a bias in the estimations of τ_D and α could occur at low or at high concentrations of an mEGFP-tagged chimera. Therefore, we checked for the impact of the mEGFP-HEXIM1 concentration on the determination of diffusive properties. The ACF amplitude together with the effective FCS volume provides an estimation of the concentration of mEGFP-tagged chimeras in the nucleus (see Materials and Methods for more details). We observed that at low (<10–20 nM) or high concentrations (>500 nM), a few acquisitions gave rise to out-of-range parameter values. The values with unphysical diffusion coefficient for nuclear protein ($D > 10^3$ $\mu m^2/s$ or $\alpha > 1.5$, indicating active transports not reported for nuclear proteins) were removed from the analysis. For the remaining values, we noticed a tendency toward an increase of both τ_D and, to a lesser extent, α with an increasing concentration (Fig. 1, *C* and *D*). Within the physiological range of expression (between 20 and 100 nM), some variability was observed, more pronounced for τ_D than for α. The latter appears to be the most robust parameter. We chose to stick to 20–100 nM HEXIM1 concentrations, a range shown to functionally inhibit P-TEFb activity (40), to avoid artifacts related to overexpression.

HEXIM1 interaction with 7SK snRNA strongly determines its subdiffusive behavior

HEXIM1 is a hub interacting with several proteins, such as P-TEFb, or RNA, such as the 7SK small nuclear RNA (snRNA), and forms ribonucleoproteic (RNP) complexes such as the large P-TEFb/HEXIM1/7SK complex (22). We investigated whether the interaction between HEXIM1 and 7SK RNA modified HEXIM1 diffusion. mEGFP was fused to the N-terminal part of HEXIM1 as were most tags in the seminal work from Michels et al (22). Still, we found a similar molecular diffusion for N-terminal and C-terminal tagging of wild-type HEXIM1 (data not shown). We first co-expressed a 7SK RNA form deprived of the third hairpin loop (7SK d6, lacking nucleotides 173–270), which was reported to stabilize the large P-TEFb complex by losing its interaction with several heterogenous nuclear RNPs (23). HEXIM1 residence time τ_D and anomaly coefficient α were respectively enhanced and decreased upon 7SKd6 expression (Fig. 2 *A*), although none of the modification reached statistical significance ($p = 0.12$ and 0.24, respectively; Table S2). Conversely, 7SK RNA knock-down by siRNA significantly decreased the HEXIM1 τ_D to 636 ± 100 μs and increased α up to 0.78 ± 0.02. These results indicated that the interaction between HEXIM1 and 7SK snRNA at least partly explained the subdiffusion of HEXIM1.

To further investigate this, we took advantage of various HEXIM1 mutants reported in the literature. Replacement of the KHRR sequence (amino acids 152–155) by the ILAA sequence suppresses the binding of HEXIM1 to 7SK and P-TEFb as evidenced both by two-hybrid experiments and GST pull downs (22). Although the KHRR sequence overlaps the HEXIM1 nuclear localization sequence, the HEXIM1 ILAA mutant was nuclear with a pattern similar to the wild-type tagged protein (Fig. 2 *B*). This mutant provided a strong change in HEXIM1 diffusive properties with an increased α value of 0.83 ± 0.01 and a decreased τ_D value of 530 ± 33 μs (Fig. 2 *C*). The α value for the ILAA mutant was close to that of mEGFP-mNeptune (0.84), although it had a higher τ_D, which suggested that the ILAA mutation strongly decreased HEXIM1 subdiffusion.

HEXIM1 forms highly anisotropic dimers (41). We subsequently checked the impact of HEXIM1 dimerization on its diffusion. Substitution of leucines 287 and 294 by arginines (thereafter called "2LR" mutation) strongly impairs HEXIM1 dimerization but not its interaction with 7SK RNA and P-TEFb (42). HEXIM1 2LR mEGFP was distributed homogenously in the nucleoplasm and was even present in the nucleoli when compared to wild-type HEXIM1 or the other mutants. Its diffusion was intermediate between HEXIM1 ILAA and mEGFP-mNeptune, with an α coefficient above 0.8, although both mutants had a higher τ_D when compared to mEGFP.

Altogether, our results show that HEXIM1 subdiffusion depends on its interaction with 7SK snRNA, either directly or indirectly via partner proteins interacting with 7SK snRNA. We therefore assessed whether the core components of P-TEFb, which are among the best described partners of HEXIM1, are involved in HEXIM1 subdiffusion.

P-TEFb constrains HEXIM1 diffusion

We made use of siRNAs and of mutants deficient for their interaction with P-TEFb to elucidate this process. We first took advantage of HEXIM1 mutations impairing its

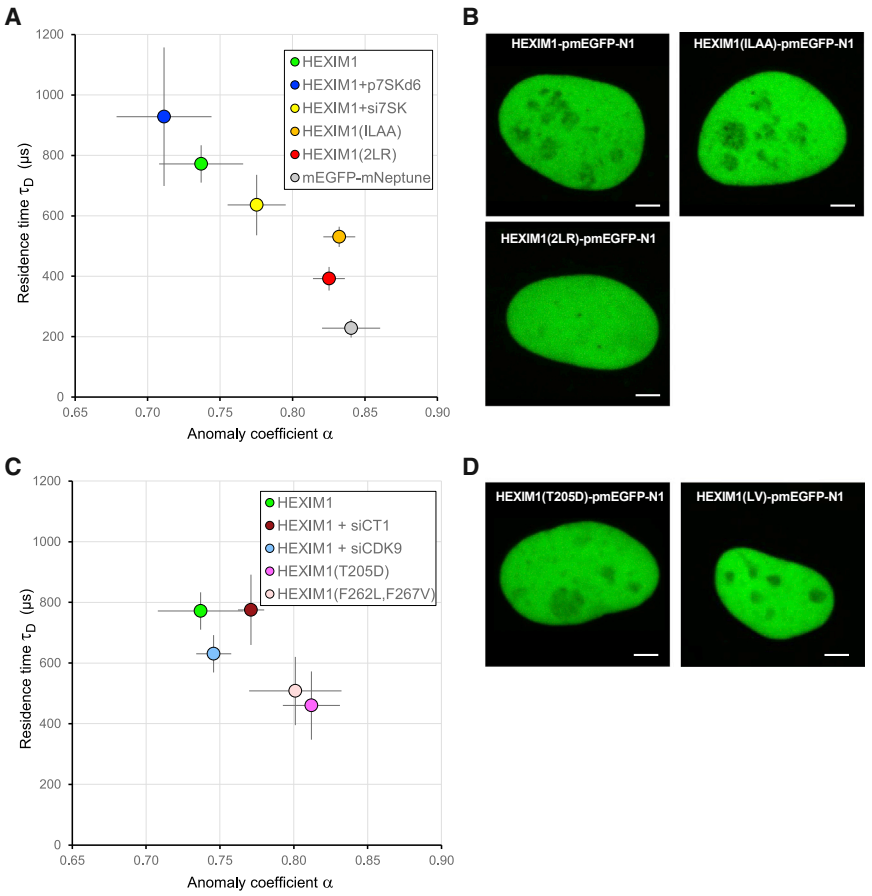

FIGURE 2 HEXIM1 anomalous diffusion features are controlled by its interactions with 7SK and P-TEFb. (*A*) The diffusion of wild-type mEGFP-HEXIM1 in the nucleoplasm was measured after co-transfection either with a plasmid encoding for the 7SKd6 version or with siRNA directed against 7SK. In parallel, cells were transfected with mEGFP-tagged mutant versions of HEXIM1, namely ILAA and 2LR. These mutants have been reported to lose their ability to interact with the 7SK RNA or their capacity to dimerize, respectively. mEGFP-mNeptune is used as a control. After calculations from the ACF curves, residence times τ_D were plotted as a function of anomaly coefficient α (mean $\pm$ SD; n $>$ 125 for each condition). Statistical significance for the various parameters and conditions is displayed in Table S2. (*B*) Representative pictures show relatively homogenous nuclear localization of both wild-type and ILAA mutant, with a weaker signal in regions corresponding to nucleoli; the 2LR mutant signal is homogenous and present even in the nucleoli. Scale bars, 2 μm. (*C*) The importance of P-TEFb for HEXIM1 anomalous diffusion was investigated by using siRNA directed against either CT1 or CDK9. In parallel, cells were transfected with mEGFP-tagged HEXIM1 mutants T205D and F262L/F267V described to have lost their interaction with P-TEFb. After calculations from the ACF curves, residence times τ_D were plotted as a function of anomaly coefficient α (mean $\pm$ SD; n $>$ 125 for each condition). (*D*) Representative pictures display quite homogenous nuclear localization of T205D and LV (for F262L/F267V), similar to that of wild-type HEXIM1 shown in (*B*). Scale bars, 2 μm. To see this figure in color, go online.

interaction with P-TEFb without affecting dimerization. The conserved PYNT sequence (amino acids 202–205) was identified by GST pull down and co-immunoprecipitation as critical in HEXIM1 binding to both P-TEFb subunits (CT1 and CDK9) (22). Another key motif for HEXIM1-P-TEFb interaction included two phenylalanine residues at positions 262 and 267, required for HEXIM1 interaction with CT1 in a two-hybrid assay (43). Remarkably, both mEGFP-tagged HEXIM1 mutants T205D and LV (for mutations F262L + F267V) showed a greatly enhanced diffusion, with both a higher α and a decreased τ_D when compared to wild-type HEXIM1 (Fig. 2 *C*). Both HEXIM1 mutants displayed a homogenous nuclear pattern, similar to that observed with the wild-type tagged protein (Fig. 2 *D*).

We then used siRNAs to knock down the expression of either of the two P-TEFb components, CT1 and CDK9. In both cases, α was not significantly modified with regard to the control condition, yet siRNAs directed against CDK9 induced a decrease in HEXIM1 τ_D (631 $\pm$ 61 μs) (Fig. 2 *C*). It has to be noted that siRNAs did not completely extinguish CT1 or CDK9 expression in our experiments (Fig. S2, *A* and *B*). In this context, CT1 residual expression, as well as the compensatory formation of P-TEFb complexes with cyclin T2A/B (44), may explain the absence of the effect of CT1 siRNAs.

To sum up, we show that HEXIM1 mutants deficient for interactions with 7SK RNA and P-TEFb are affected in their anomalous diffusion with respect to wild-type HEXIM1 and that the progressive suppression of these interactions releases HEXIM1, which subsequently diffuses freely.

Simulations support a model in which the ratios between distinct oligomers control HEXIM1 apparent anomalous diffusion

We then aimed at creating a model representative of how molecular interactions impact on mobility. For that purpose, we simulated autocorrelation curves from a code based on the Monte Carlo method (36).

To model the alterations of HEXIM1 diffusion with respect to its interactions and based on the fact that HEXIM1 exists in various different complexes in vivo, free or complexed with several molecules (7SK RNA and P-TEFb), we generated simulations with two or three populations of molecules. Interactions between HEXIM1, 7SK, and P-TEFb occur within periods much longer than τ_D

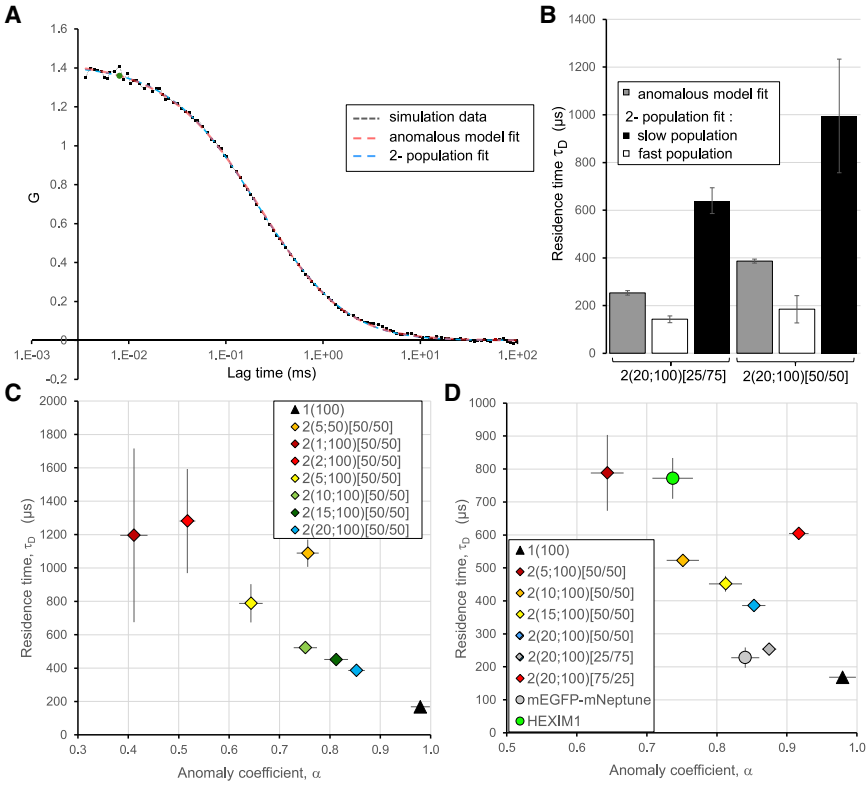

FIGURE 3 Simulations with two populations can be grasped with an anomalous model. (*A*) ACFs (*black dots*) obtained from a simulation with two subpopulations diffusing at 20 and 100 $\mu m^2/s$ and representing 25 and 75% of the whole population, respectively, can be fitted with both an anomalous model (*blue dashed line*) and a two-population model (*red dashed line*). (*B*) Simulations were generated with two populations respectively diffusing at 20 and 100 $\mu m^2/s$, present either in proportions 25%/75% or 50%/50%. Gray bars correspond to the residence times τ_D calculated with the anomalous model (mean ± SD). The same simulations were fitted with a two-population model, and the residence times τ_D of the fast and slow populations (*white* and *black bars*, respectively) display a greater variability. (*C*) Simulations generated with one (*triangle*) or two (*diamonds*) population(s) were analyzed with the anomalous model, and residence times τ_D are plotted as a function of the anomaly coefficient α (mean ± SD). (*D*) Simulations generated with two populations present in various proportions were analyzed with the anomalous model, and residence times τ_D are plotted as diamonds as a function of the anomaly coefficient α (mean ± SD). mEGFP-HEXIM1 and free mEGFP experimental values are represented as controls. To see this figure in color, go online.

measured in our FCS experiments (dissociation rates between 1 and 10 s^{-1} have been reported (45)). We therefore considered in our model that individual molecules did not change their diffusion behavior during their transit through the focal volume and could be modeled at first with independent freely diffusing particles of distinct diffusion coefficients, corresponding to distinct oligomers. It was previously described that a single ACF could be modeled as well by an anomalous model as by a Brownian two-component model (39). We further investigated this concept of apparent anomaly generated by mixing two or three populations.

To make the reading more fluent, we will use the following nomenclature for each simulation: $N(A_1 \ldots A_N)[X_1 \ldots X_N]$ corresponds to N populations diffusing at respective $A_1 \ldots A_N$ diffusion coefficients (in $\mu m^2/s$) and present in proportions $X_1 \ldots X_N$ percentage of the total population. Because nuclear proteins classically exhibit mean diffusion coefficients around tens of $\mu m^2/s$, we limited our simulations to diffusion values one order of magnitude bigger or smaller (i.e., from 1 to 100 $\mu m^2/s$). We started our simulations with a reductionist approach, and by combining two free populations of distinct diffusion coefficients, we confirmed that the resulting ACF could be fitted by an anomalous model as well as with a two-population model (Fig. 3 *A*). Yet, fitting the simulation curves with a two-population model resulted in τ_D displaying a larger variance when compared to the anomalous model (Fig. 3 *B*). We then modified the diffusion coefficient ratios between equimolar populations. When decreasing the speed of the slow fraction, the mean diffusion was progressively decreased, with a higher τ_D and a decreased α reaching 0.4 with the 2 (1;100)[50/50] condition (Fig. 3 *C*). It should be noted that a broad difference in the diffusion coefficients of the two populations increased the residuals of the ACF fit (Fig. S3 *A*) that led to a decrease in the precision of both α and τ_D as reported by the increased mean ± SD (Fig. 3 *C*). A shift in the proportion of the two populations had a strong effect on τ_D and the 2 (20;100)[25/75] condition proved to approximate quite well mEGFPx2 diffusion (Fig. 3 *D*).

Strikingly, the inclusion of a third distinct population resulted in a broader range of α and τ_D compatible with wild-type HEXIM1 diffusion (Fig. 4 *A*). The condition 3 (5,20;100)[33/33/33] was characterized by an α equal to 0.74 and a τ_D of 740 μs (Fig. 4 *A*; Table S3), very close to the experimental values for wild-type HEXIM1. Besides, the SDs in both α and τ_D were similar to the ones of our experimental data. Please note also that the ACF fit residuals were improved when compared to the 2 (5;100)[50/50] condition (Fig. S3, *A* and *B*).

We subsequently studied the impact of parameters, such as coefficient values, populations ratios, and concentrations, upon the calculated diffusive parameters to extract

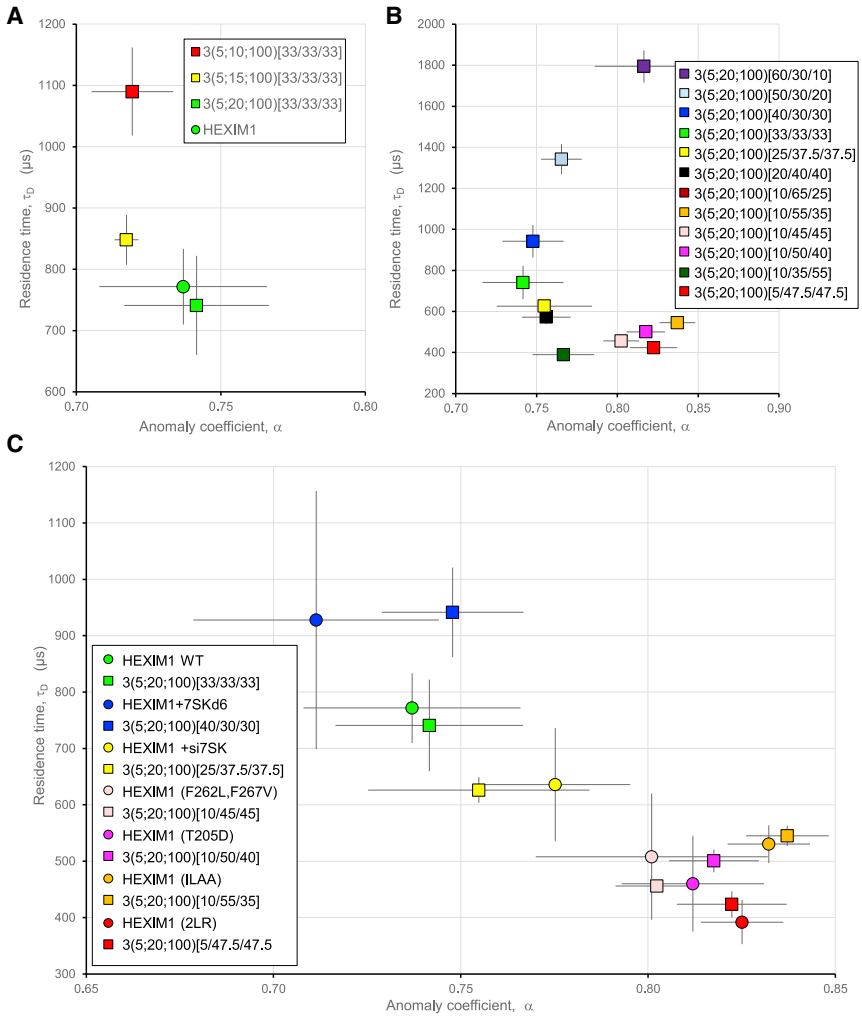

FIGURE 4 Simulations support a model in which the ratios between distinct oligomers controls HEXIM1 anomalous diffusion. (*A* and *B*). Simulations generated with three populations of varying diffusion coefficients (*A*) and present in various proportions (*B*) were analyzed with the anomalous model, and residence times τ_D are plotted as a function of the anomaly coefficient α (mean ± SD). (*C*) Simulations generated with several populations can recapitulate the anomalous diffusion of HEXIM1 and the modifications that changes in interactome induce, as reported in Fig. 2. Experimental values are represented as circles. Squares correspond to three-population simulations. The color code pairs up the experimental data with the corresponding closest simulation. To see this figure in color, go online.

as much information as possible from our model. We observed that τ_D is highly dependent on the characteristics of the most abundant population (Fig. 4 *B*). When varying the concentration ratio between two populations, we also noticed that the apparent α resulting from the mixture of two populations in the condition 2 (5;100)[P1/P3] ranged from 0.74 to 0.85 with the lowest values at nearly equimolar concentrations (Fig. S4 *A*). As observed with two populations, fitting the 3-population simulation curves with a 3-population model gave a great variability when compared to the anomalous model (Fig.S4 *B*) and bad population proportion assessment (data not shown). This fact highlights the drawbacks of the n population model and supports using the anomalous model as a less error-prone method. We finally investigated the impact of the molecular concentration on the diffusion assessment and found similar mean values under the different conditions (Fig. S4 *C*). Still, increasing the overall concentration improved the accuracy of the analysis as illustrated by the reduced mean ± SD.

We then performed a statistical analysis to compare experimental results with simulations (Table S4). A color code was used to match each experimental result with the closest simulation (Fig. 4 *C*). Because our experiments pointed to 7SK and P-TEFb bindings to HEXIM1 as brakes for HEXIM1 diffusion, we postulated that the slow fraction in our model corresponds to the HEXIM1/7SK/P-TEFb oligomer. The expression of 7SKd6 is meant to enhance HEXIM1 recruitment by P-TEFb and can actually be mimicked by a slight increase in the slow population proportions ([40/30/30]). τ_D reached 942 μs in this simulation, though α was not affected ($\alpha = 0.75$). Conversely, the use of si7SK decreases the slow population proportion and was recapitulated by the 3 (5,20;100)[25/37.5/37.5] ratios. The F262L/F267V and T205D mutants lose their interactions with P-TEFb and are presumably further impaired in the formation of the slow complex. The F262L/F267V mutant was best approximated by the simulation 3 (5,20;100)[10/45/45]. And the T205D mutant characteristics were recapitulated with high statistical significance by

all simulations with a slow population reduced to 5 or 10% of the total population. A more pronounced shift in anomaly is obtained with the 2LR HEXIM1 mutant, which loses most of its dimerization capacities and consequently its ability to oligomerize with its partners, and is recapitulated by the highest reduction of the slow fraction (3 (5,20;100)[5/47.5/47.5]). Finally, the ILAA HEXIM1 mutant which is highly impaired in its interaction with both 7SK and P-TEFb but not in its capacity to dimerize matches in the simulations a situation in which the fraction of the intermediate population increased, namely 3 (5,20;100)[10/55/35].

Altogether, these data show that anomalous diffusion can be recapitulated with multicomponent simulations. They also suggest that the apparent anomalous behavior of HEXIM1 may correspond to a binding equilibrium.

DISCUSSION

From biochemical reactions to biological functions, molecular interactions play a key role and have been a focus of attention of the research community. How molecules find their targets in biological systems remains a key issue, especially in the transcription field. In this study, we focused on a complex of RNA and proteins, well described to assemble and dissociate in vivo. We used the P-TEFb and its regulators HEXIM1 and 7SK RNA to investigate the relationship between interactions and diffusion.

Several loss-of-interaction mutants then allowed us to illustrate the contribution of partners to HEXIM1 subdiffusion. Interestingly, loss of interaction with P-TEFb thanks to the T205D mutant greatly shifted HEXIM1 toward a more Brownian diffusion, close to that of mEGFP. The more severe ILAA mutant, which is impaired for its interaction with both 7SK RNA and P-TEFb, displayed a similar behavior, suggesting that 7SK and P-TEFB are the main determinants for HEXIM1 subdiffusion. In addition, impairment of HEXIM1 dimerization with the 2LR mutant also increased the HEXIM1 anomaly coefficient, although this mutant has been reported to still interact with 7SK RNA and P-TEFb (42). This indicates that, beyond the possibility for HEXIM1 to interact with its partners, its diffusion relies on the formation of functional oligomers able to interact with other proteins or DNA during the transcription pause release process.

Because HEXIM1 can be free or complexed with several molecules (7SK RNA and P-TEFb) in cells, we generated simulations with two or three populations of particles with distinct diffusion coefficients. Given that interactions within these complexes have been reported to last much longer than HEXIM1 residence time in FCS, we postulated that no change in the diffusion coefficient occurred during the transit through the observation volume. Thanks to these simulations, we show that the mere combination of freely diffusing distinct oligomers creates a population behavior that can be perceived as anomalous. This point had been touched on by the team of the late Jörg Langowski, who concluded in their study (39) that the anomalous model could serve to assess a degree of subdiffusion, alternately to a two-component model. Later on, it was also reported that simulations of asymmetric diffusion or binding/unbinding events can be well fit with the anomalous model (46,47). In such cases, α and τ_D parameters lose their true physical meanings while becoming helpful tools to compare several conditions. With regard to HEXIM1, comparison of simulations with experimental results suggests an equilibrium between a slow population in complex with P-TEFb and 7SK, a fast population with free HEXIM1 molecules and an intermediate population, which may correspond to HEXIM1 engaged in other complexes or in weak interactions.

Our study reinforces the concept of α as a helpful and robust indicator of altered diffusion. This also raises a critical and intriguing question (i.e., to which extent and in which regimes anomalous diffusion can be a phenomenological reflection of free population combinations or is a truly scale-dependent phenomenon). Both phenomena may also coexist and contribute to the apparent anomalous diffusion. Future works will be aimed at elucidating this issue, which may offer a new view on molecular diffusion in biology.

By fitting the ACF of both the 3-population simulations or experimental data, we show that a fitting method with three populations gives rise to frequent aberrant results in terms of diffusion speeds and proportions between the populations. This lack of robustness of fitting methods when several parameters can be adjusted is, by the way, a known caveat, which has encouraged over the last years the development of nonfitting methods in biophysics (48). Moreover, in cells, in which the exact number of populations of distinct molecular compositions cannot be known and is at best

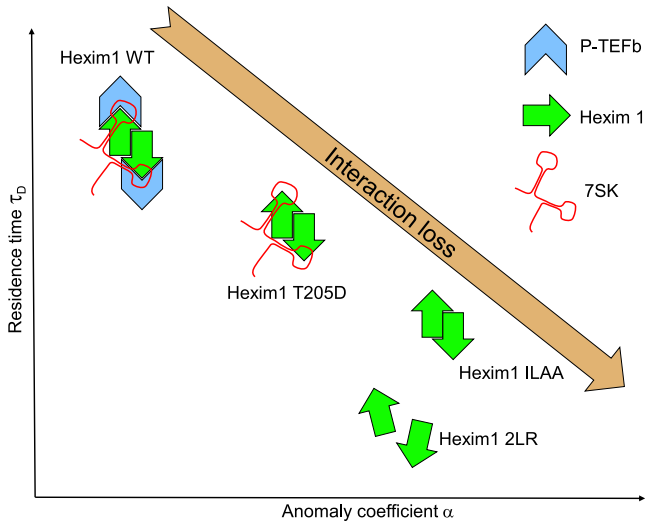

FIGURE 5 An overview of HEXIM1 changes in diffusion depending on its interactions with its partners. This scheme sums up the information on variations of HEXIM1 diffusive properties in distinct oligomers. HEXIM1 is represented as a green arrow, P-TEFb is represented as a blue arrowhead, and 7SK RNA is represented as a red ribbon. To see this figure in color, go online.

approximated, such a fitting is highly error prone, especially because the number of collected photons is restricted. The anomalous model could account for most of the features in our data, and the global α represents the most reliable phenomenological tool to measure the diffusion of mixed molecular populations in cells, without a priori knowledge or assumptions. In that way, it constitutes a helpful tool to assess and understand interactions in cells.

Our results, which show that HEXIM1 oligomerization with 7SK RNA and P-TEFb controls HEXIM1 anomalous diffusion (Fig. 5), support the concept of interactions as main determinants of anomaly in the nucleoplasm. Previous studies had highlighted the importance of strong interactions with receptor scaffolds or nuclear matrix in restraining diffusion (49–51). To the best of our knowledge, it is the first time that α was demonstrated as a useful tool to reveal loss of interactions for soluble small molecules in the nucleoplasm.

In addition to P-TEFb regulation, HEXIM1 stabilizes p53 (52) and is involved in complexes dubbed HEXIM1-DNA-PK paraspeckle components ribonucleoprotein complex (53). It would be interesting to understand if the various HEXIM1 functions require distinct confinements and if putative distinct subpopulations of HEXIM1 molecules can be caught in particular conditions. More globally, our study shows that the anomaly coefficient can be used as a simple tool to report on molecular interactions involved in various important biological questions.

We also show that the diffusion of mEGFP-mNeptune can be recapitulated with simulations of a predominant fast population mixed with a slowed down fraction. The existence of two mEGFP populations with distinct diffusion coefficients in the nucleoplasm had already been suggested by Enrico Gratton's team (54).

Finally, one should note that the spatial organization of the nucleoplasm, despite the lack of true compartments in the nucleus, can be achieved via biophysical mechanisms including phase separation (55). P-TEFb activity was very recently proposed to be regulated via such a mechanism (56). In this context, weak and dynamic interactions, such as those occurring in the transcriptional pause release, can drive the nucleation of structures with reduced dimensionality (57,58). Whether HEXIM1 is affected by or contributes to this process and whether it impacts its activity will be the focus of future investigations.

Recently, we have developed a fluorescence lifetime imaging Förster resonance energy transfer-based correlation method to quantify the clusters of interactions between P-TEFb and RNA polymerase II as well as with histones, which we used to report the larger cluster areas of P-TEFb mutants lacking interaction with RNA polymerase (29). Conversely, in the current study, we used FCS to report changes in interactions via the measurement of diffusion. We therefore feel that the gap between techniques measuring interactions and those reporting diffusion is getting filled, so that reaction-diffusion systems in biology can be better understood.

SUPPORTING MATERIAL

Supporting Material can be found online at https://doi.org/10.1016/j.bpj.2019.09.019.

AUTHOR CONTRIBUTIONS

A.F., M.G.-P., A.L., G.B., and L.H. designed research. A.F., M.G.-P., A.L., D.C., M.H. and G.B. performed experiments. A.F., M.-G.P., A.L., C.L.N., O.B., M.L., T.W., B.V., G.B., and L.H. analyzed and interpreted the data. A.F., A.L., T.W., B.V., G.B., and L.H. wrote the manuscript.

ACKNOWLEDGMENTS

We thank all members of our team for their help and comments. Calculations were performed using high-performance computing resources from Direction du NUMérique Centre de Calcul de l'Université de Bourgogne. This work was supported by Agence Nationale de la Recherche (Dynamic-12-BSV5-0018-02), Region ''Hauts de France'' (Contrat Plan Etat Région Photonics4 Society and I-PRIMER), EquipEX ImaginEx BioMed (Programme d'Investissements d'Avenir/Region Hauts de France), Ministerial Funding, CNRS, and a contract Nikon-CNRS. T.W. was supported by a grant from the Singapore Ministry of Education (MOE2016-T2-2-121).

REFERENCES

1. Meldi, L., and J. H. Brickner. 2011. Compartmentalization of the nucleus. *Trends Cell Biol.* 21:701–708.
2. Cremer, T., and M. Cremer. 2010. Chromosome territories. *Cold Spring Harb. Perspect. Biol.* 2:a003889.
3. Bancaud, A., S. Huet, …, J. Ellenberg. 2009. Molecular crowding affects diffusion and binding of nuclear proteins in heterochromatin and reveals the fractal organization of chromatin. *EMBO J.* 28:3785–3798.
4. Ellis, R. J., and A. P. Minton. 2003. Cell biology: join the crowd. *Nature.* 425:27–28.
5. Izeddin, I., V. Récamier, …, X. Darzacq. 2014. Single-molecule tracking in live cells reveals distinct target-search strategies of transcription factors in the nucleus. *ELife.* 3. Published online June 12:2014. https://doi.org/10.7554/eLife.02230.
6. Matsuda, H., G. G. Putzel, …, I. Szleifer. 2014. Macromolecular crowding as a regulator of gene transcription. *Biophys. J.* 106:1801–1810.
7. Feder, T. J., I. Brust-Mascher, …, W. W. Webb. 1996. Constrained diffusion or immobile fraction on cell surfaces: a new interpretation. *Biophys. J.* 70:2767–2773.
8. Höfling, F., and T. Franosch. 2013. Anomalous transport in the crowded world of biological cells. *Rep. Prog. Phys.* 76:046602.
9. Guigas, G., and M. Weiss. 2008. Sampling the cell with anomalous diffusion - the discovery of slowness. *Biophys. J.* 94:90–94.
10. Malchus, N., and M. Weiss. 2010. Elucidating anomalous protein diffusion in living cells with fluorescence correlation spectroscopy-facts and pitfalls. *J. Fluoresc.* 20:19–26.
11. Saxton, M. J. 2007. A biological interpretation of transient anomalous subdiffusion. I. Qualitative model. *Biophys. J.* 92:1178–1191.
12. Guigas, G., C. Kalla, and M. Weiss. 2007. Probing the nanoscale viscoelasticity of intracellular fluids in living cells. *Biophys. J.* 93:316–323.
13. Balbo, J., P. Mereghetti, …, R. C. Wade. 2013. The shape of protein crowders is a major determinant of protein diffusion. *Biophys. J.* 104:1576–1584.

14. Ando, T., and J. Skolnick. 2010. Crowding and hydrodynamic interactions likely dominate in vivo macromolecular motion. *Proc. Natl. Acad. Sci. USA.* 107:18457–18462.
15. Zustiak, S. P., R. Nossal, and D. L. Sackett. 2011. Hindered diffusion in polymeric solutions studied by fluorescence correlation spectroscopy. *Biophys. J.* 101:255–264.
16. Almassalha, L. M., A. Tiwari, …, V. Backman. 2017. The global relationship between chromatin physical topology, fractal structure, and gene expression. *Sci. Rep.* 7:41061.
17. Langowski, J. 2008. Protein-protein interactions determined by fluorescence correlation spectroscopy. *Methods Cell Biol.* 85:471–484.
18. Beck, M., A. Schmidt, …, R. Aebersold. 2011. The quantitative proteome of a human cell line. *Mol. Syst. Biol.* 7:549.
19. Core, L. J., A. L. Martins, …, J. T. Lis. 2014. Analysis of nascent RNA identifies a unified architecture of initiation regions at mammalian promoters and enhancers. *Nat. Genet.* 46:1311–1320.
20. Michels, A. A., V. T. Nguyen, …, O. Bensaude. 2003. MAQ1 and 7SK RNA interact with CDK9/cyclin T complexes in a transcription-dependent manner. *Mol. Cell. Biol.* 23:4859–4869.
21. Nguyen, V. T., T. Kiss, …, O. Bensaude. 2001. 7SK small nuclear RNA binds to and inhibits the activity of CDK9/cyclin T complexes. *Nature.* 414:322–325.
22. Michels, A. A., A. Fraldi, …, O. Bensaude. 2004. Binding of the 7SK snRNA turns the HEXIM1 protein into a P-TEFb (CDK9/cyclin T) inhibitor. *EMBO J.* 23:2608–2619.
23. Van Herreweghe, E., S. Egloff, …, T. Kiss. 2007. Dynamic remodelling of human 7SK snRNP controls the nuclear level of active P-TEFb. *EMBO J.* 26:3570–3580.
24. Liu, W., Q. Ma, …, M. G. Rosenfeld. 2013. Brd4 and JMJD6-associated anti-pause enhancers in regulation of transcriptional pause release. *Cell.* 155:1581–1595.
25. Shelton, S. B., N. M. Shah, …, B. Xhemalçe. 2018. Crosstalk between the RNA methylation and histone-binding activities of MePCE regulates P-TEFb activation on chromatin. *Cell Rep.* 22:1374–1383.
26. Michels, A. A., and O. Bensaude. 2018. Hexim1, an RNA-controlled protein hub. *Transcription.* 9:262–271.
27. Krieger, J. W., A. P. Singh, …, T. Wohland. 2015. Imaging fluorescence (cross-) correlation spectroscopy in live cells and organisms. *Nat. Protoc.* 10:1948–1974.
28. Albrecht, D., C. M. Winterflood, and H. Ewers. 2015. Dual color single particle tracking via nanobodies. *Methods Appl. Fluoresc.* 3:024001.
29. Bidaux, G., C. Le Nézet, …, L. Héliot. 2018. FRET image correlation spectroscopy reveals RNAPII-independent P-TEFb recruitment on chromatin. *Biophys. J.* 114:522–533.
30. Kim, S. A., K. G. Heinze, and P. Schwille. 2007. Fluorescence correlation spectroscopy in living cells. *Nat. Methods.* 4:963–973.
31. Mailfert, S., Y. Hamon, …, D. Marguet. 2017. A user's guide for characterizing plasma membrane subdomains in living cells by spot variation fluorescence correlation spectroscopy. *Methods Cell. Biol.* 139:1–22.
32. Krueger, B. J., C. Jeronimo, …, D. H. Price. 2008. LARP7 is a stable component of the 7SK snRNP while P-TEFb, HEXIM1 and hnRNP A1 are reversibly associated. *Nucleic Acids Res.* 36:2219–2229.
33. Haaland, R. E., C. H. Herrmann, and A. P. Rice. 2005. siRNA depletion of 7SK snRNA induces apoptosis but does not affect expression of the HIV-1 LTR or P-TEFb-dependent cellular genes. *J. Cell. Physiol.* 205:463–470.
34. Schaub, E. 2012. F2Cor: fast 2-stage correlation algorithm for FCS and DLS. *Opt. Express.* 20:2184–2195.
35. Qian, H., and E. L. Elson. 1991. Analysis of confocal laser-microscope optics for 3-D fluorescence correlation spectroscopy. *Appl. Opt.* 30:1185–1195.
36. Wohland, T., R. Rigler, and H. Vogel. 2001. The standard deviation in fluorescence correlation spectroscopy. *Biophys. J.* 80:2987–2999.
37. Bajar, B. T., E. S. Wang, …, J. Chu. 2016. Improving brightness and photostability of green and red fluorescent proteins for live cell imaging and FRET reporting. *Sci. Rep.* 6:20889.
38. Cranfill, P. J., B. R. Sell, …, D. W. Piston. 2016. Quantitative assessment of fluorescent proteins. *Nat. Methods.* 13:557–562.
39. Wachsmuth, M., W. Waldeck, and J. Langowski. 2000. Anomalous diffusion of fluorescent probes inside living cell nuclei investigated by spatially-resolved fluorescence correlation spectroscopy. *J. Mol. Biol.* 298:677–689.
40. Czudnochowski, N., C. A. Bösken, and M. Geyer. 2012. Serine-7 but not serine-5 phosphorylation primes RNA polymerase II CTD for P-TEFb recognition. *Nat. Commun.* 3:842.
41. Dulac, C., A. A. Michels, …, O. Bensaude. 2005. Transcription-dependent association of multiple positive transcription elongation factor units to a HEXIM multimer. *J. Biol. Chem.* 280:30619–30629.
42. Li, Q., J. P. Price, …, D. H. Price. 2005. Analysis of the large inactive P-TEFb complex indicates that it contains one 7SK molecule, a dimer of HEXIM1 or HEXIM2, and two P-TEFb molecules containing Cdk9 phosphorylated at threonine 186. *J. Biol. Chem.* 280:28819–28826.
43. Verstraete, N., A. Kuzmina, …, O. Bensaude. 2014. A Cyclin T1 point mutation that abolishes positive transcription elongation factor (P-TEFb) binding to Hexim1 and HIV tat. *Retrovirology.* 11:50.
44. Peng, J., Y. Zhu, …, D. H. Price. 1998. Identification of multiple cyclin subunits of human P-TEFb. *Genes Dev.* 12:755–762.
45. Schulte, A., N. Czudnochowski, …, M. Geyer. 2005. Identification of a cyclin T-binding domain in Hexim1 and biochemical analysis of its binding competition with HIV-1 Tat. *J. Biol. Chem.* 280:24968–24977.
46. Milon, S., R. Hovius, …, T. Wohland. 2003. Factors influencing fluorescence correlation spectroscopy measurements on membranes: simulations and experiments. *Chem. Phys.* 288:171–186.
47. Tsekouras, K., A. P. Siegel, …, S. Pressé. 2015. Inferring diffusion dynamics from FCS in heterogeneous nuclear environments. *Biophys. J.* 109:7–17.
48. Leray, A., C. Spriet, …, L. Héliot. 2011. Quantitative comparison of polar approach versus fitting method in time domain FLIM image analysis. *Cytometry A.* 79:149–158.
49. Weigel, A. V., B. Simon, …, D. Krapf. 2011. Ergodic and nonergodic processes coexist in the plasma membrane as observed by single-molecule tracking. *Proc. Natl. Acad. Sci. USA.* 108:6438–6443.
50. Bronshtein, I., E. Kepten, …, Y. Garini. 2015. Loss of lamin A function increases chromatin dynamics in the nuclear interior. *Nat. Commun.* 6:8044.
51. Sungkaworn, T., M. L. Jobin, …, D. Calebiro. 2017. Single-molecule imaging reveals receptor-G protein interactions at cell surface hot spots. *Nature.* 550:543–547.
52. Lew, Q. J., Y. L. Chia, …, S. H. Chao. 2012. Identification of HEXIM1 as a positive regulator of p53. *J. Biol. Chem.* 287:36443–36454.
53. Morchikh, M., A. Cribier, …, M. Benkirane. 2017. HEXIM1 and NEAT1 long non-coding RNA form a multi-subunit complex that regulates DNA-mediated innate immune response. *Mol. Cell.* 67:387–399.e5.
54. Hinde, E., F. Cardarelli, …, E. Gratton. 2010. In vivo pair correlation analysis of EGFP intranuclear diffusion reveals DNA-dependent molecular flow. *Proc. Natl. Acad. Sci. USA.* 107:16560–16565.
55. Erdel, F., and K. Rippe. 2018. formation of chromatin subcompartments by Phase separation. *Biophys. J.* 114:2262–2270.
56. Lu, H., D. Yu, …, Q. Zhou. 2018. Phase-separation mechanism for C-terminal hyperphosphorylation of RNA polymerase II. *Nature.* 558:318–323.
57. Woringer, M., and X. Darzacq. 2018. Protein motion in the nucleus: from anomalous diffusion to weak interactions. *Biochem. Soc. Trans.* 46:945–956.
58. Chong, S., C. Dugast-Darzacq, …, R. Tjian. 2018. Imaging dynamic and selective low-complexity domain interactions that control gene transcription. *Science.* 361:eaar2555.